CONVECTIVE FLUX SCHEMES FOR HIGH-REYNOLDS-NUMBER COMPRESSIBLE FLOWS

Enda Dimitri V. Bigarella
Instituto Tecnológico de Aeronáutica, CTA/ITA, São José dos Campos, BRAZIL
enda.bigarella@ig.com.br

Edson Basso and João Luiz F. Azevedo
Instituto de Aeronáutica e Espaço, CTA/IAE, São José dos Campos, BRAZIL
basso@iae.cta.br, azevedo@iae.cta.br

Abstract. *This paper presents the effects of some convective flux computation schemes on boundary layer and shocked flow solutions. For such study, centered and upwind convective flux computation schemes are discussed. The centered Jameson scheme plus explicitly added artificial dissipation terms is considered. Three artificial dissipation models are addressed in the paper. The 2nd-order Roe flux-difference-splitting upwind scheme is also discussed. Some schemes require property reconstruction to achieve second-order accuracy in space, which is obtained with an extended multidimensional limited MUSCL interpolation method. It is observed that artificial dissipation terms may strongly modify the flow solution.*

Keywords: *CFD, boundary layers, flux computation*

1. Introduction

The main interest in the present paper is to assess some 2nd-order-accurate flux calculation methods suitable for typical aerospace applications. A Jameson centered (Jameson et al., 1981) and a Roe flux-difference splitting upwind schemes (Roe, 1981) are available. In the centered case, explicit addition of artificial dissipation terms is required to control nonlinear instabilities in the numerical solution. Both a scalar and a matrix version of a switched second- and fourth-difference model are available (Mavriplis, 1990; Turkel and Vatsa, 1994), as well as the Convective Upwind Split Pressure (CUSP) model (Jameson, 1995). The CUSP and Roe schemes require property reconstruction in the control volume face to achieve 2nd-order accuracy in space. A multidimensional limited (Barth and Jespersen, 1989) MUSCL-type reconstruction scheme is currently used. An extension of original multidimensional limiter formulation is also proposed. A computationally cheaper and robust integration of the limited MUSCL-reconstructed schemes is also proposed, which allows for large computational resource savings while maintaining the expected level of accuracy. Typical aerospace flows are currently presented to address the effect of the flux computation scheme at shock-wave and boundary-layer flows.

2. Theoretical Formulation

The flows of interest in the present context are modeled by the 3-D compressible Reynolds-averaged Navier-Stokes (RANS) equations. These equations can be written in dimensionless form, assuming a perfect gas, as

$$\frac{\partial \mathbf{Q}}{\partial t} + \nabla \cdot (\mathbf{P}_e - \mathbf{P}_v) = 0 \,, \qquad \mathbf{Q} = \left[\begin{array}{ccccc} \rho & \rho u & \rho v & \rho w & e \end{array} \right]^{\mathrm{T}} . \tag{1}$$

In this definition, $\mathbf{Q}$ is the dimensionless vector of conserved variables, where ρ is the fluid density, $\mathbf{v} = \{u, v, w\}$ is the Cartesian velocity vector and e is the fluid total energy per unit of volume. In Eq. (1), the $\mathbf{P}_e$ term is the dimensionless inviscid flux vector, and $\mathbf{P}_v$ is the dimensionless viscous flux vector. These vectors are given in details in Bigarella and Azevedo, 2005. Advanced eddy-viscosity turbulence models suitable for external aerodynamics applications, that are able to predict flow separation with acceptable levels of accuracy, are also available.

3. Numerical Formulation

The formulation of the method is obtained by an integration of the flow equations in a finite volume with the application of Gauss' theorem within each control volume. The implementation uses a cell-centered, face-based structure and the code can use hybrid meshes composed by tetrahedra, hexahedra, wedges and pyramids. The integration in time is performed using a 2nd-order 5-stage Runge-Kutta type scheme. The time step for each volume is calculated for a constant CFL number. A full approximation storage (FAS) multigrid scheme is available in order to accelerate the convergence to steady state. In order to improve the multigrid algorithm, a full multigrid (FMG) method is adopted, in which the simulations start at the coarsest grid level until reaching the finest grid. The coarse mesh levels are generated by an agglomeration technique. More details on the multigrid and agglomeration algorithm, as well as on the numerical formulation, can be found in Bigarella et al., 2004, and Bigarella and Azevedo, 2005.

4. Spatial Discretization

Centered schemes require the explicit addition of artificial dissipation terms in order to control nonlinear instabilities that may arise in the flow simulation. A description of the available models is presented in the forthcoming subsections. The upwind scheme and the reconstruction formulation are also discussed.

4.0.1 Mavriplis Scalar Switched Model (MAVR)

The centered spatial discretization of the convective fluxes, $\mathbf{C}_i$, in this scheme is proposed by Jameson et al., 1981. The artificial dissipation operator is built by a switch of undivided Laplacian and bi-harmonic operators. In regions of high property gradients, the bi-harmonic operator is turned off in order to avoid oscillations. In smooth regions, the undivided Laplacian operator is turned off in order to maintain 2nd-order accuracy. The expression for the artificial dissipation operator is given by

$$\mathbf{D}_i = \sum_{k=1}^{nb} \left\{ \frac{1}{2} \left(\mathbf{A}_m + \mathbf{A}_i \right) \left[\epsilon_2 \left(\mathbf{Q}_m - \mathbf{Q}_i \right) - \epsilon_4 \left(\nabla^2 \mathbf{Q}_m - \nabla^2 \mathbf{Q}_i \right) \right] \right\} , \tag{2}$$

where m represents the neighbor of the i-th element, attached to the k-th face, and nb is the total number of neighbors of the i-th control volume. Furthermore,

$$\nabla^2 \mathbf{Q}_i = \sum_{k=1}^{nb} \left[\mathbf{Q}_m - \mathbf{Q}_i \right] , \quad \epsilon_2 = K_2 \max\left(\nu_i, \nu_m \right) , \quad \epsilon_4 = \max\left(0, K_4 - \epsilon_2 \right) , \quad \nu_i = \frac{\sum_{m=1}^{nb} \left| p_m - p_i \right|}{\sum_{m=1}^{nb} \left[p_m + p_i \right]} . \tag{3}$$

In this work, K_2 and K_4 are assumed equal to $1/4$ and $3/256$, respectively. The $\mathbf{A}_i$ matrix coefficient in Eq. (2) is replaced by a scalar coefficient (Mavriplis, 1990) such as $A_i = \sum_{k=1}^{nf} \left[\left| \mathbf{v}_k \cdot \mathbf{S}_k \right| + a_k \left| \mathbf{S}_k \right| \right]$.

4.0.2 Matrix Switched Model (MATD)

The formulation for the matrix model is similar to the previously described one for the MAVR model, except for the definition of the $\mathbf{A}_i$ terms. In this case, the flux Jacobian matrices (Turkel and Vatsa, 1994) are used instead of the scalar term. The $\mathbf{A}_i$ term, re-interpreted for the present cell-centered, face-based finite-volume framework, can be written as $\mathbf{A}_i = \sum_{k=1}^{nf} |\mathbf{A}_k||\mathbf{S}_k|$, where

$$\begin{aligned} |\mathbf{A}_k| &= |\lambda_3| \mathbf{I} + \left[\frac{1}{2} \left(|\lambda_1| + |\lambda_2| \right) - |\lambda_3| \right] \left(\frac{\gamma - 1}{a_k^2} \mathbf{E}_1 + \mathbf{E}_2 \right) + \frac{1}{2 a_k} \left(|\lambda_1| - |\lambda_2| \right) \left[\mathbf{E}_3 + \left(\gamma - 1 \right) \mathbf{E}_4 \right] , \\ |\lambda_1| &= \max\left(|v_n + a|, \, V_n \lambda \right) , \quad |\lambda_2| = \max\left(|v_n - a|, \, V_n \lambda \right) , \quad |\lambda_3| = \max\left(|v_n|, \, V_l \lambda \right) , \quad \lambda = |v_n| + a . \end{aligned} \tag{4}$$

In the previous definitions, $v_n = \mathbf{v} \cdot \mathbf{n}$ is the normal velocity component, where $\mathbf{n}$ is the unit area vector, and $\mathbf{E}_n$ arrays are given in Bigarella and Azevedo, 2005. Furthermore, V_n and V_l are used near stagnation and/or sonic lines to avoid zero artificial dissipation. The recommended values for these limiters are $V_n = 0.25$ and $V_l = 0.025$.

In the finite difference context in which the matrix-based artificial dissipation model is presented (Turkel and Vatsa, 1994), its implementation is very cheap due to the advantageous form of the $|\mathbf{A}_k|$ matrix in terms of vector multiplications. However, the artificial dissipation model in the current context is calibrated with the use of integrated coefficients, such as in MAVR model. Therefore, the advantageous form of the $|\mathbf{A}_k|$ matrix cannot be used because a surface integral of the matrix coefficient must be evaluated. This is the straightforward extension of the scalar option to the matrix one, here termed $MATD_{sf}$. The finite difference-like option, named $MATD_{fd}$, in which the attractive form of the scaling matrix is used, can be readily obtained by replacing the $\frac{1}{2} \left(\mathbf{A}_m + \mathbf{A}_i \right)$ coefficient in Eq. (2) by the $|\mathbf{A}_k||\mathbf{S}_k|$ scaling matrix. Another option in which the advantageous form of the scaling matrix is kept while still using an integrated coefficient, though in a nonconservative fashion, can also be obtained, here termed $MATD_{nc}$ (Bigarella and Azevedo, 2005).

4.0.3 Convective Upwind and Split Pressure Scheme (CUSP)

Previously, the scalar and matrix-valued artificial dissipation terms have been constructed considering differentials in the conserved property array. For the CUSP model, the artificial dissipation terms are instead chosen as a linear combination of the conserved property array and the flux vectors. The second-order accurate CUSP model artificial dissipation term can be given by

$$\mathbf{D}_i = \sum_{k=1}^{nf} \left[\frac{1}{2} \alpha^* a_k |\mathbf{S}_k| \left(\mathbf{Q}_R - \mathbf{Q}_L \right) + \frac{1}{2} \beta \left(\mathbf{P}_{e_R} - \mathbf{P}_{e_L} \right) \cdot \mathbf{S}_k \right] , \tag{5}$$

and

$$\alpha = \begin{cases} |M_n| & \text{if } |M_n| \geq \epsilon \\ \frac{1}{2}\left(\epsilon + \frac{M_n^2}{\epsilon}\right) & \text{if } |M_n| < \epsilon \end{cases} \quad , \quad \beta = \text{sign}(M_n)\min\left(1, \max\left(0, 2|M_n| - 1\right)\right) \; , \quad \alpha = \alpha^* + \beta M_n \; . \tag{6}$$

In these equations, $M_n = v_n/a$ is the Mach number in the face normal direction, and ϵ is a threshold control in order to avoid zero artificial dissipation near stagnation lines. The L and R subscript represent reconstructed neighboring properties of the k-th face. The definitions for such properties is presented in the forthcoming section about the MUSCL reconstruction scheme. It is important to remark here that face properties are computed using the Roe average procedure (Roe, 1981).

The centered spatial discretization of the convective fluxes can be built using reconstructed properties, here termed $CUSP_{rec}$ scheme. This does not seem to be the approach chosen by other CUSP users (Jameson, 1995; Swanson et al., 1998). In these references, reconstructed properties apparently are used only to build the dissipation terms, and constant property distribution is assumed to build the convective terms. This approach is named $CUSP_{ctt}$ in the present context.

4.1 Upwind Roe Flux-Difference Splitting Scheme (f ROE)

The upwind discretization in the present context is performed by the Roe flux-difference splitting method (Roe, 1981). For this scheme, the numerical flux in the k-th face can be written as

$$\mathbf{P}_{ek} = \frac{1}{2}\left(\mathbf{P}_{e_L} + \mathbf{P}_{e_R}\right) - \frac{1}{2}\left|\widetilde{\mathbf{A}}_k\right|\left(\mathbf{Q}_R - \mathbf{Q}_L\right) \; , \tag{7}$$

where $\left|\widetilde{\mathbf{A}}_k\right|$ is the Roe matrix associated with the k-th face normal direction, defined as $\left|\widetilde{\mathbf{A}}\right|\left(\mathbf{Q}_R - \mathbf{Q}_L\right) = |\lambda_i|\,\delta_i\,\mathbf{r}_i$. In this formulation, $|\lambda_i|$ represents the absolute values of the eigenvalues associated with the Euler equations, given as $|\mathbf{\Lambda}| = \left[\begin{array}{ccccc} |v_n| & |v_n| & |v_n| & |v_n + a| & |v_n - a| \end{array}\right]^{\mathrm{T}}$. Similarly, $\mathbf{r}_i$ represents the associated eigenvectors to the right (Bigarella and Azevedo, 2005). The δ_i term represents the element of projection of the property jump at the interface over the system eigenvectors, which is defined as $\mathbf{\Delta} = \mathbf{L}\left[\begin{array}{ccccc} \Delta\rho & \Delta(\rho\,u) & \Delta(\rho\,v) & \Delta(\rho\,w) & \Delta e \end{array}\right]^{\mathrm{T}}$, where the rows of $\mathbf{L}$ represents the left eigenvectors. Properties in the volume faces are also computed using the Roe average procedure.

In the classical form in which the f ROE scheme is presented, named $fROE_{cla}$, (Eq. 7), the underlining argument is the numerical flux concept. Therefore, each time the numerical flux is built, the inherent numerical dissipation is also evaluated. In an explicit Runge-Kutta-type multistage scheme, this fact means that the Roe matrix defined in Eq. (7) is computed in all stages. The present authors rather understand the f ROE scheme as the sum of a centered convective flux, as used in the CUSP scheme, and an upwind-biased numerical dissipation contribution, that is given by the subtracted term in the right-hand side of Eq. (7). Therefore, the attractive cheaper alternate dissipation computation in the multi-stage scheme, as already used for the switched artificial dissipation schemes (Bigarella and Azevedo, 2005), can also be extended for the upwind flux computation, termed $fROE_{alt}$.

4.2 MUSCL Reconstruction

The linear reconstruction of properties is achieved through a MUSCL scheme (Bigarella and Azevedo, 2005), in which the property at the interface is obtained through a limited extrapolation using the cell properties and their gradients. In order to perform such reconstruction at any point inside the control cell, the following expression is used for a generic element, q, of the conserved variable vector, $\mathbf{Q}$: $q\left(x, y, z\right) = q_i + \nabla q \cdot \vec{r}$, where (x, y, z) is a generic point in the i-th cell; q_i is the discrete value of the generic property q in the i-th cell, which is attributed to the cell centroid; ∇q is the gradient of property q; and $\vec{r}$ is the distance of the cell centroid to that generic point.

The expressions for the reconstructed properties in the k-th face can be written as $(q_L)_k = q_i + \psi_i \nabla q_i \cdot \vec{r}_{ki}$ and $(q_R)_k = q_m + \psi_m \nabla q_m \cdot \vec{r}_{km}$, where i and m represent the i-th and m-th cells, respectively; ψ_i and ψ_m represent the limiters in these cells; and $\vec{r}_{ki}$ and $\vec{r}_{km}$ are the distance vectors from these cell centroids to the k-th face centroid. The 1st-order CUSP or f ROE schemes can be readily obtained by setting the limiter value to zero.

4.3 Limiter Formulations

The limiter computation workload is a very expensive task, amounting to more than half of an iteration computational effort in the present code. Therefore, the idea of freezing the limiter along with the dissipation operator at some stages of the multistage time-stepping scheme is very attractive in terms of large computational resource savings.

4.3.1 Barth and Jespersen Multidimensional Limiter Implementation ($MUSCL_{BJ}$)

In this method, the extrapolated property in the k-th face of the i-th cell is bounded by the maximum and minimum values over the i-th cell centroid and its neighbor cell centroids (Barth and Jespersen, 1989). This TVD interpretation can

be mathematically written as $q_i^- \leq (q_i)_k \leq q_i^+$, where $q_i^+ = \max(q_i, q_{neighbors})$ and $q_i^- = \min(q_i, q_{neighbors})$. The Barth and Jespersen limiter computation in the i-th cell is initiated by collecting the minimum, q_i^-, and the maximum, q_i^+, values for the generic q variable in the i-th cell and its neighbor centroids. A limiter is computed at each j-th vertex of the control volume as

$$\psi_j(\Phi) = \begin{cases} \min\left(1, num_{BJ}^+/den_{BJ}\right) & \text{, if } den_{BJ} > 0\,, \\ \min\left(1, num_{BJ}^-/den_{BJ}\right) & \text{, if } den_{BJ} < 0\,, \end{cases} \tag{8}$$

where $den_{BJ} = (q_i)_j - q_i$, $num_{BJ}^+ = q_i^+ - q_i$ and $num_{BJ}^- = q_i^- - q_i$. The j-th vertex property is extrapolated from the i-th cell centroid with the aid of $(q_i)_j = q_i + \nabla q \cdot \vec{r}_{ji}$. Barth and Jespersen argue that the use of the property in the cell vertices gives the best estimate of the solution gradient in the cell. The limiter value for the i-th control volume, ψ_i, is finally obtained as the minimum value of the limiters computed for the vertices.

4.3.2 General Multidimensional Limiter Implementation ($MUSCL_{ge}$)

The current extension of the 1-D limiters to the multidimensional case is based on the work of Barth and Jespersen (Barth and Jespersen, 1989). The Barth and Jespersen limiter is a complete limiter implementation in itself, and it has some advantages as well as disadvantages. This extension is aimed at allowing for the user the choice of any desired limiter formulation, and at solving some disadvantages of the $MUSCL_{BJ}$ limiter. The limiter options that are available in the present context are the *minmod*, *superbee* and *van Albada* limiters (Hirsch, 1991). One should aknowledge that the *minmod* and *superbee* limiters require the evaluation of maximum and minimum functions, which characterizes these limiters as discontinuous. The *van Albada* limiter, on the other hand, is continuous.

The difficulty in implementing a TVD method in a multidimensional unstructured scheme is related to how to defined the gradient ratio of adjacent cell, Φ. A generalization of Φ to the k-th face of the i-th cell of an unstructured grid (Bigarella and Azevedo, 2005) can be given by

$$\Phi = (\Phi_i)_k = \frac{\left(q_i^{\pm} - q_i\right)/|\vec{r}_{mi}|}{\left((q_i)_k - q_i\right)/|\vec{r}_{ki}|}\,, \tag{9}$$

where the k-th face is shared by the i-th and m-th cells; and the extrapolated property in the face, $(q_i)_k$, is given by $(q_i)_k = q_i + \nabla q_i \cdot \vec{r}_{ki}$.

In this formulation, considering a quasi-uniform grid, in which $|\vec{r}_{mi}| \approx 2|\vec{r}_{ki}|$, we can write

$$\frac{1}{|\vec{r}_{mi}|}\left(q_i^{\pm} - q_i\right) \approx \frac{1}{2|\vec{r}_{ki}|}\left(q_i^{\pm} - q_i\right) = \frac{1}{|\vec{r}_{ki}|}\left(\frac{q_i^{\pm} + q_i}{2} - q_i\right) = \frac{1}{|\vec{r}_{ki}|}\left(q_k^{\pm} - q_i\right)\,, \tag{10}$$

where $q_k^{\pm}$ is the maximum and minimum properties obtained at the centroid of the faces that compose the i-th control volume. The $q_k^{\pm}$ variable can be mathematically defined as $q_k^{\pm} = \max / \min(q_i, q_{faces})$, where the property in the faces, q_{faces}, is the arithmetic average of the properties in the neighboring cells. The multidimensional gradient ratio for an unstructured grid face can be finally obtained as

$$\Phi = \begin{cases} num^+/den & \text{, if } den > 0\,, \\ num^-/den & \text{, if } den < 0\,, \end{cases} \tag{11}$$

where $den = (q_i)_k - q_i$, $num^+ = q_k^+ - q_i$, $num^- = q_k^- - q_i$. Also, $\Phi = 1$ for $den = 0$.

The advantage of the gradient ratio definition in Eq. (11) is that it can be directly used in any other limiter definition. It can also be used to recast the original Barth and Jespersen limiter formulation, as previously discussed, with a slight modification though. As also discussed, the original Barth and Jespersen limiter uses extrapolated properties in the nodes to build the gradient ratio, while extrapolated properties in the faces are preferred in the current implementation. Considering the Barth and Jespersen vertex choice in the current gradient ratio definition (Eq. 11), it can be observed that

$$\Phi^{(correct)} = \frac{num^{\pm}/|\vec{r}_{ki}|}{den/|\vec{r}_{ji}|} = \frac{|\vec{r}_{ji}|}{|\vec{r}_{ki}|}\left(\frac{num^{\pm}}{den}\right) = \frac{|\vec{r}_{ji}|}{|\vec{r}_{ki}|}\Phi^{(implemented)} \Rightarrow \Phi^{(implemented)} = \frac{|\vec{r}_{ki}|}{|\vec{r}_{ji}|}\Phi^{(correct)}\,. \tag{12}$$

In this formulation, the mesh intervals $|\vec{r}_{ki}|/|\vec{r}_{ji}|$ cannot be canceled as in Eq. (10), and their ratio is lower than one, which results is an implemented gradient ratio smaller than the correct one. This difference yields in smaller limiter values, which can be interpreted as an undesired increase of diffusivity in the limiter implementation. This issue can be avoided with the use of extrapolated face properties, as proposed in Eqs. (9) and (10).

5. Results and Discussion

For this study, the influence of the numerical schemes in shock-wave resolution is assessed with a 1-D shock-tube problem, as well as transonic inviscid flows about a typical supercritical airfoil. Also, boundary layer flows are addressed through subsonic laminar flows about a flat plate configuration, with Reynolds number $Re = 10^5$ and Mach number $M_\infty = 0.254$.

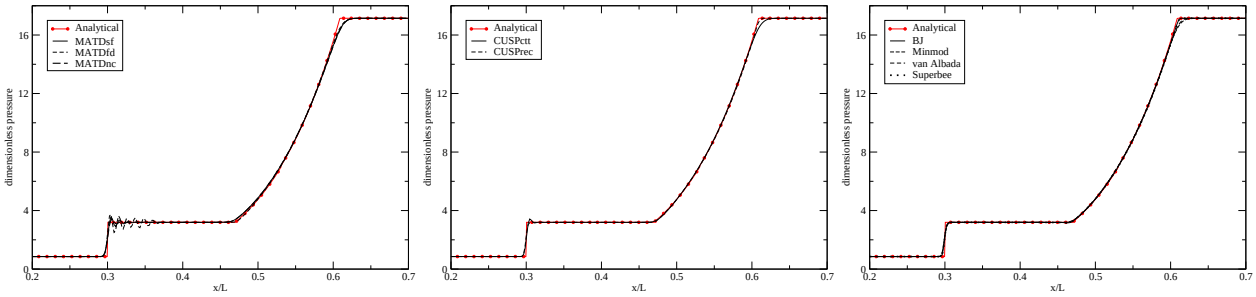

(a) MATD. (b) CUSP. (c) MUSCL.

Figure 1. Property distributions along the shock tube obtained with different flux computation schemes.

5.1 1-D Shock Tube Results

Numerical results are compared to the analytical solution for this problem. The initial dimensionless density condition for the left half part of the shock tube is $\rho_{ini}^{L} = 1$, whereas on the right half, $\rho_{ini}^{R} = 20$. The three possible implementation forms of the MATD artificial dissipation method are currently assessed. Dimensionless pressure distributions along the tube longitudinal axis are presented in Fig. 1. One can clearly observe in this figure that all MATD options allow for pre- and post-discontinuity oscillation to build up. The less correct $MATD_{fd}$ option presents much larger oscillations, whereas the $MATD_{nc}$ presents the lowest levels. The $MATD_{fd}$ and $MATD_{nc}$ options require about 30% less computational time than the $MATD_{sf}$ formulation for this test case.

For CUSP results, the *van Albada* limiter is used in the currently proposed multidimensional limiter implementation. Swanson et al., 1998 argue that the original $CUSP_{ctt}$ formulation does not nominally provide oscillation-free shocked-flow results. The current authors believe this behavior is due to the use of constant properties in the cells to computate the centered convective fluxes. The use of reconstructed properties in the faces may rather overcome such limitation. These arguments are corroborated by the CUSP pressure results presented in Fig. 1. It can be observed that the original $CUSP_{ctt}$ formulation allows oscillation to build-up near discontinuities, while the currently proposed $CUSP_{rec}$ option prevents such undesired behavior. $CUSP_{rec}$ implementation requires less than 10% additional computational time than $CUSP_{ctt}$ in this case.

The $fROE_{cla}$ implementation option for the Roe scheme is compared to the currently proposed $fROE_{alt}$ implementation. Limiter settings are exactly the same as used for the previous CUSP scheme simulations. Pressure distributions for the Roe scheme are not presented because no differences between $fROE_{cla}$ and $fROE_{alt}$ options can be observed. The $fROE_{cla}$ scheme, however, is about twice more expensive than the currently proposed $fROE_{alt}$ implementation.

Finally, the original Barth and Jespersen multidimensional limiter ($MUSCL_{BJ}$) is compared to the currently proposed generic multidimensional implementation ($MUSCL_{ge}$). The *minmod*, *van Albada* and *superbee* limiters are considered in order to demonstrate the capability of the current multidimensional reconstruction scheme to handle various limiter types. For this study, the $fROE_{alt}$ scheme is used with limiter computations at alternate stages of the Runge-Kutta scheme. Pressure results for the previous limiter options are shown in Fig. 1. It is clear that the current multidimensional reconstruction scheme does allow for the use of various limiter formulations. No oscillatory behavior in the numerical solutions can be observed in all presented results. The comparison with the analytical solution is also good, with the *superbee* limiter presenting crisper discontinuities, as expected, due to its less diffusive formulation. As already discussed, the *Barth and Jespersen* limiter recast the *superbee* limiter in the $0 \leq \Phi \leq 1$ range, in a 1-D case, and its results are virtually equal to the latter limiter ones. The *van Albada* limiter results lie within the more- and the less-diffusive *minmod* and *superbee* limiters, respectively, as expected.

5.2 2-D Airfoil Results

Transonic inviscid flows about the Boeing A4 supercritical airfoil (Bigarella and Azevedo, 2005) are assessed. In these analyses, the MATD model stands for the $MATD_{nc}$ option; the CUSP model is actually the $CUSP_{rec}$ option with the van Albada limiter computed at alternate time-stepping scheme stages; and the f ROE scheme represents the $fROE_{alt}$ implementation with the same previous CUSP limiter settings. Three C-type grids, with 100×24, 150×40 and 255×64 cells over the profile and along the normal direction, respectively, are used. The freestream Mach number is $M_{\infty} = 0.768$ and the angle of attack is $\alpha = 1.4$ deg.

Pressure coefficient distributions over the profile obtained with different meshes and flux computation schemes are presented in Fig. 2. One can observe that MAVR presents considerable variations in the shock wave position as the grid is refined. More consistent results can be obtained with the MATD model. The CUSP and f ROE schemes present even more consistent results, and the variations in the numerical solution with grid refinement are much lower, with the CUSP scheme presenting slightly better results.

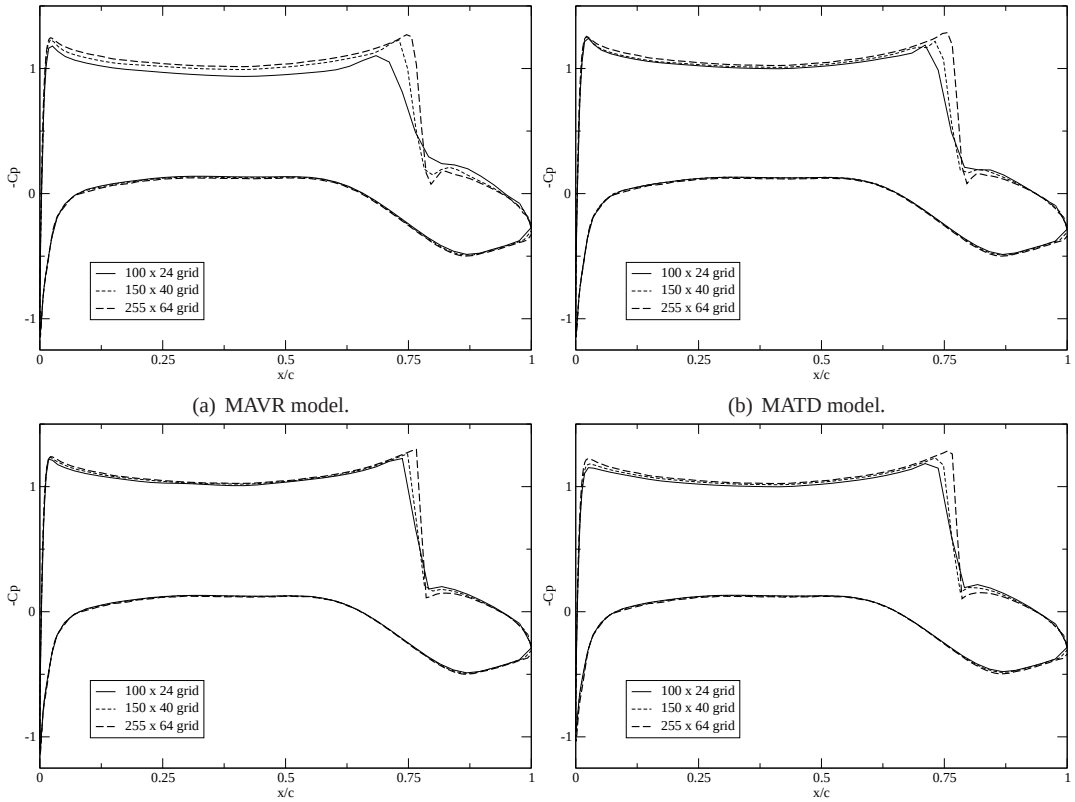

(a) MAVR model. (b) MATD model.

(c) CUSP model. (d) f ROE scheme.

Figure 2. Wall Cp distributions over the supercritical airfoil obtained with different flux computation schemes and computational grids.

5.2.1 MUSCL Results

The original Barth and Jespersen multidimensional limiter ($MUSCL_{BJ}$) is compared to the currently proposed generic multidimensional implementation ($MUSCL_{ge}$). Cp distributions and residue histories for this study are presented in Fig. 3. No oscillatory behavior in the numerical solutions can be observed in all presented results. It is interesting to observe, however, in the residue histories in Fig. 3(b) that the *minmod*, *Barth and Jespersen* and *superbee* limiters present residue stall, due to their discontinuous formulation. The continuous *van Albada* option, on the contrary, allows for automatic residue convergence.

5.3 Flat Plate Results

It is known that some schemes may have some influence in boundary layer flow solutions (Bigarella and Azevedo, 2005). The present effort has also been motivated by an anomaly found in subsonic flat-plate boundary layers, more precisely, in the bend of the boundary layer profile. Hence, three consecutively refined grids have been generated for this flow case. For the present case, different number of cells inside the boundary layer, namely 10, 20 and 40 cells, are considered. Figure 4 presents boundary layer results obtained with the previously described computational grids, compared to the Blasius analytical solution. The flux schemes considered in this figure are the same as used in the previous 2-D airfoil subsection. One should observe that the f ROE, MATD and CUSP schemes guarantee the correct solution with all tested grids. The MAVR centered scheme presents an anomaly in the bend of the boundary layer profile for the grids with a smaller number of points in the layer. The oscillation, nevertheless, decreases with the increasing number of such points.

6. Concluding Remarks

The paper presents results obtained with a finite volume code developed to solve the RANS equations over aerospace configurations. Several flux computation schemes are considered in the paper. The convective fluxes on the volume faces are computed by either a centered scheme plus explicitly added artificial dissipation terms, or the 2nd-order Roe upwind scheme. Three artificial dissipation models are considered to compute the numerical diffusion for the centered scheme. A scalar and a matrix version of a switched model, and the CUSP scheme, are used. Several implementation approaches for

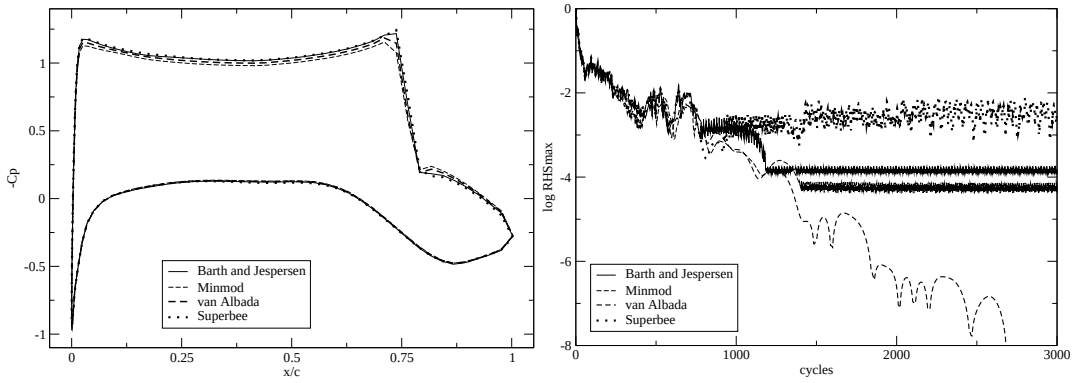

(a) Cp distributions. (b) Residue histories.

Figure 3. Simulation results for the supercritical airfoil obtained with different limiter implementations.

such methods are considered in the paper.

Multidimensional MUSCL interpolation techniques are used in order to achieve 2nd-order accuracy for schemes which require property reconstruction. An extension to the work of Barth and Jespersen is currently proposed and verified. With such extension, various limiter formulations can be used within the multidimensional unstructured code structure. Cheaper integration of the Roe and CUSP schemes, as well as the limiter construction, is achieved through computation at alternate stages of the Runge-Kutta time-stepping procedure, while still maintaining the quality level of the solutions.

Comparisons of numerical boundary layers for a flat plate laminar flow with the corresponding theoretical Blasius solution show the level of accuracy os the present formulation. It is observed that the scalar artificial dissipation model presents a very large dependency on the grid density and topology, while other more refined methods are less sensitive to that. The ability of the flux computation schemes in calculating shock waves in the solution is also assessed. It is observed that more consistent solutions can be obtained with the Roe and CUSP schemes, to which small variations with grid refinement are verified. The scalar artificial dissipation model is not so effective in these analyses, and a considerable dependency of the numerical solution with the grid configuration is observed.

7. Acknowledgments

The authors would like to acknowledge Conselho Nacional de Desenvolvimento Científico e Tecnológico, CNPq, which partially supported the project under the Integrated Project Research Grant No. 501200/2003-7. The authors also acknowledge Dr. P. Batten of Metacomp Technologies for his insights on the development of the limiter formulations here presented.

8. References

Barth, T. J. and Jespersen, D. C., 1989, The Design and Application of Upwind Schemes on Unstructured Meshes, “27th AIAA Aerospace Sciences Meeting”, AIAA Paper No. 89-0366, Reno, NV.

Bigarella, E. D. V. and Azevedo, J. L. F., 2005, A Study of Convective Flux Computation Schemes for Aerodynamic Flows, “43rd AIAA Aerospace Sciences Meeting and Exhibit”, AIAA Paper No. 2005-0633, Reno, NV.

Bigarella, E. D. V., Basso, E., and Azevedo, J. L. F., 2004, Centered and Upwind Multigrid Turbulent Flow Simulations with Applications to Launch Vehicles, “22nd AIAA Applied Aerodynamics Conference and Exhibit”, AIAA Paper No. 2004-5384, Providence, RI.

Hirsch, C., 1991, “Numerical Computation of Internal and External Flows Volume 2: Computational Methods for Inviscid and Viscous Flows”, chapter 21. Wiley, Chichester.

Jameson, A., 1995, Analysis and Design of Numerical Schemes for Gas Dynamics 2. Artificial Diffusion and Discrete Shock Structure, “International Journal of Computational Fluid Dynamics”, Vol. 5, pp. 1–38.

Jameson, A., Schmidt, W., and Turkel, E., 1981, Numerical Solution of the Euler Equations by Finite Volume Methods Using Runge-Kutta Time-Stepping Schemes, “14th AIAA Fluid and Plasma Dynamics Conference”, AIAA Paper 81-1259, Palo Alto, CA.

Mavriplis, D. J., 1990, Accurate Multigrid Solution of the Euler Equations on Unstructured and Adaptive Meshes, “AIAA Journal”, Vol. 28, No. 2, pp. 213–221.

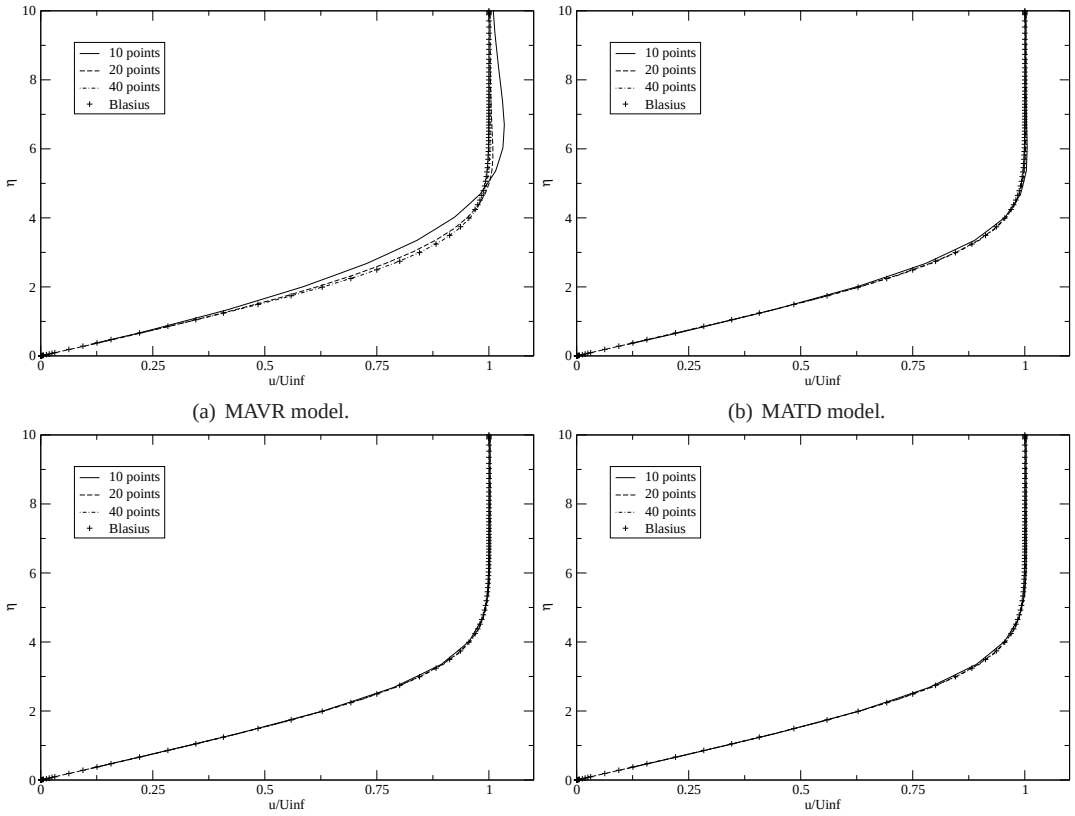

(a) MAVR model. (b) MATD model.

(c) CUSP model. (d) f ROE scheme.

Figure 4. Laminar boundary layer profiles over a flat plate obtained with different flux computation schemes and computational grids.

Roe, P. L., 1981, Approximate Riemann Solvers, Parameter Vectors, and Difference Schemes, "Journal of Computational Physics", Vol. 43, No. 2, pp. 357–372.

Swanson, R. C., Radespiel, R., and Turkel, E., 1998, On Some Numerical Dissipation Schemes, "Journal of Computational Physics", Vol. 147, No. 2, pp. 518–544.

Turkel, E. and Vatsa, V. N., 1994, Effect of Artificial Viscosity on Three-Dimensional Flow Solutions, "AIAA Journal", Vol. 32, No. 1, pp. 39–45.